

低温超音速喷涂团聚铁粒子沉积的 SPH 模拟

侯根良¹, 许欣², 袁晓静¹

(1. 第二炮兵工程学院 501 室, 西安 710025;

2. 第二炮兵装备研究院, 北京 100085)



侯根良

摘 要: 为了研究纳米团聚粒子形态对涂层特性的影响, 应用 SPH 方法研究了低温超音速火焰喷涂金属团聚粒子的沉积行为. 结果表明, 纳米粒子团聚为微米级粒子后, 基体碰撞出现了飞溅现象, 应变变化明显. 团聚粒子的等效塑性应变小于普通微米粒子, 但团聚粒子的面积扩大比大于普通微米粒子. 沉积过程中, 当超过临界沉积速度后, 金属团聚粒子与基体之间存在过渡区域, 过渡区域随粒子速度的增加而扩大.

关键词: 热喷涂; 纳米团聚粒子; 沉积特征; 数值计算

中图分类号: TG115.28 文献标识码: A 文章编号: 0253-360X(2009)05-0105-04

0 序 言

纳米团聚粒子涂层的制备是热喷涂技术发展的重要组成. 经过纳米团聚制备的涂层, 具有优良的力学性能^[1]. 为了解决纳米粉末喷涂困难的问题, 人们通过造粒将纳米粉末团聚成微米级颗粒, 然后进行喷涂. 团聚粒子内部主要靠粘结剂及物理吸附处于弱结合, 因而在沉积过程中, 团聚粒子的沉积特征对涂层的形成非常重要.

喷涂过程涉及到形变、扩散、界面, 粒子沉积时变形行为复杂, 很难直接进行观测, 采用数值模拟可以很好地观察团聚粒子沉积过程中存在的典型特征. 目前, 已有文献对普通微米粒子的沉积特征进行了数值模拟^[2-4]. 但团聚粒子的特征决定了其沉积特征必然与普通微米粒子沉积存在不同之处. SPH(smoothed particle hydrodynamics)法允许自然存在材料界面, 可以精确地描述材料复杂的本构行为, 其离散化使用固定质量的动点^[5,6]. 它的计算通常是基于离散化方程来模拟连续材料的. 但团聚粒子可以看作离散性质点的集合, SPH 方法的离散化假设就更适合于这些弱连接的质点集合, 这为描述团聚粒子的沉积奠定了理论基础.

采用 SPH 方法研究低温超音速火焰喷涂纳米金属团聚粒子的沉积行为, 分析金属团聚粒子形态对涂层构建的影响, 可以为低温超音速喷涂高性能纳米涂层提供重要的理论依据.

1 团聚粒子的 SPH 模型

SPH 是 Lagrange 型, 从计算角度来说, SPH 是把物体流场用有一定流动速度的运动质点集来描述, 每个质点就是已知流场特性的插值点, 整个问题的解通过这些质点的规则插值函数得到, 守恒方程用通量或质点内力来等效表达.

SPH 方法中, 质点近似函数为^[7]

$$\Pi^h f(x) = \int f(y)W(x-y, h)dy \quad (1)$$

式中: W 为核函数(插值核).

核函数 W 可使用辅助函数 θ 进行定义

$$W(x, h) = \frac{1}{h(x)^d} \theta(x) \quad (2)$$

式中: d 为空间维数; h 为光滑长度, 光滑长度随时间和空间变化.

SPH 方法的整个离散系统是建立在一群携带一定物理量的粒子基础上. 对于团聚粒子来讲, 其 SPH 近似, 就是通过弱结合界面的离散过程. 将弱连续粒子的守恒方程经过离散化可得到粒子求和的 SPH 形式. $W(x, h)$ 是尖峰函数, SPH 中最常用的光滑核是三次 B 样条, 定义为

$$\theta(u) = C \times \begin{cases} 1 - \frac{3}{2}u^2 + \frac{3}{4}u^3 & |u| \leq 1 \\ \frac{1}{4}(2-u) & 1 < |u| \leq 2 \\ 0 & 2 < |u| \end{cases} \quad (3)$$

式中: C 为归一化常量; u 为两个粒子之间的距离,

由空间维数确定。

2 试验与计算

低温超音速火焰喷涂过程中,粒子的速度分布为 $300 \sim 700 \text{ m/s}$, 温度为 $463 \sim 873 \text{ K}$ ^[8]。假定团聚粒子在沉积过程中,具有相同的速度,仅在飞行过程为团聚体,在碰撞基体后各粒子根据自身特性选择沉积行为。铁粒子参数为:密度 7.85 g/cm^3 ,泊松比 0.30 ,弹性模量 207 GPa ,熔点 1673 K ^[9]。计算模型中(图 1),以 SPH 粒子模拟喷涂团聚粒子的沉积,基体采用连续单元,图 1a 为计算 SPH 粒子沉积特征的 $1/4$ 几何模型,团聚粒子族的直径为 $20 \mu\text{m}$ 。SPH 粒子数量为 $32\,000$ 个,经计算单个 SPH 粒子的尺度为 47 nm 。在计算粒子界面特征时,基体也为 SPH 单元,

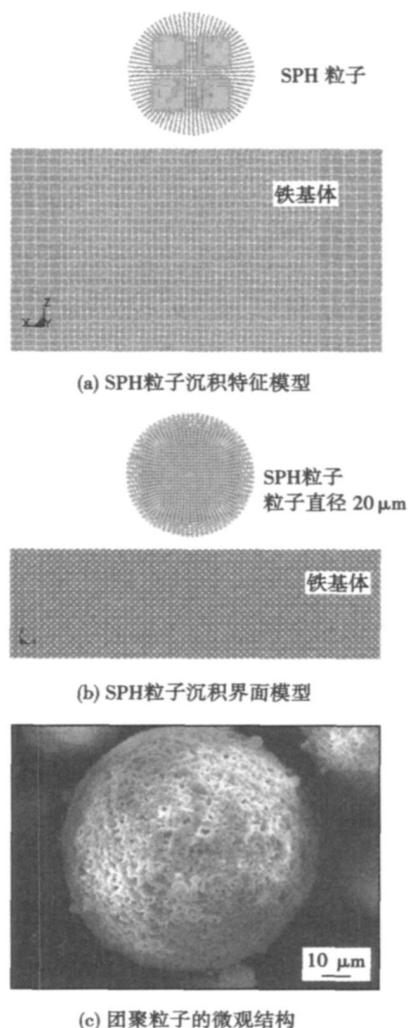


图 1 团聚粒子结构的 SPH 模型

Fig. 1 SPH model of microstructure particle in thermal spraying process

如图 1b 所示. 在进行相互比较时,所选取微米粒子的尺寸与纳米团聚粒子族的尺寸相同,均为 $20 \mu\text{m}$ 。表 1 给出了模型的基本参数和计算过程. 图 1c 为典型团聚粒子的 SEM 形貌,可以看出其团聚半径大约为 $20 \mu\text{m}$,基本上可以看作理想球体,实际喷涂过程中粒子的团聚半径可以进行控制。

表 1 模型基本参数

Table 1 Parameters of SPH model

团聚粒子数	基体粒子数	循环次数	建模时间	CPU 时间
			t_1/s	t_2/s
3.2×10^4	2.56×10^5	2 774	0.031 031	2 558

3 结果与讨论

3.1 纳米团聚粒子的典型分布特征

计算中,团聚金属粒子以 400 m/s , 500 K 撞击铁基体,图 2 给出了团聚粒子的沉积过程、团聚粒子的碰撞状态与等效塑性应变. 在团聚粒子沉积过程中(图 2a~c),当团聚粒子在低温超音速火焰中飞行时,由于受到温度特征的影响,各粒子之间的粘结剂被部分氧化掉,粒子之间成为相对孤立的集合体。

随着粒子的高速飞行,与基体碰撞并发生沉积时,粒子都会发生不同程度的飞溅现象. 图 2d~f 表明,团聚粒子撞击基体时产生巨大碰撞应力,迫使基体发生明显的有效塑性应变. 同时,沉积撞击应力还迫使团聚粒子发生破碎并产生不同程度的飞溅,而这些都与粒子的初始碰撞速度有着密切的关系。

3.2 粒子速度对基体有效塑性应变的影响

图 3 为不同速度下,相同尺寸的团聚粒子与微米粒子撞击基体时的有效塑性应变. 当粒子速度小于临界速度时,粒子的破碎很小,仍呈团聚状态,基体的塑性应变小,粒子与基体之间仅发生弹性应变,使得粒子不能够沉积在基体上. 当粒子速度超过临界沉积速度时,团聚粒子将发生破碎呈现纳米状态,但由于破碎后的粒子受到基体的反作用力,将呈现四周扩散的飞溅特征(图 2f). 团聚粒子与基体发生碰撞时,基体的有效塑性应变在同等速度下要小于同尺度微米粒子对基体撞击产生的有效塑性应变. 这表明,团聚粒子碰撞时,粒子间松散状态导致粒子在碰撞基体时产生应力方向杂化,使得粒子对基体的撞击能力下降,而应力杂化也促使粒子的破碎飞溅。

3.3 粒子速度对团聚粒子破碎面积的影响

团聚粒子的破碎面积是指在粒子没有完全软化沉积时,团聚粒子内部由于结合力较小出现单个纳米粒子的沉积面积. 图 4 为不同速度时团聚粒子沉

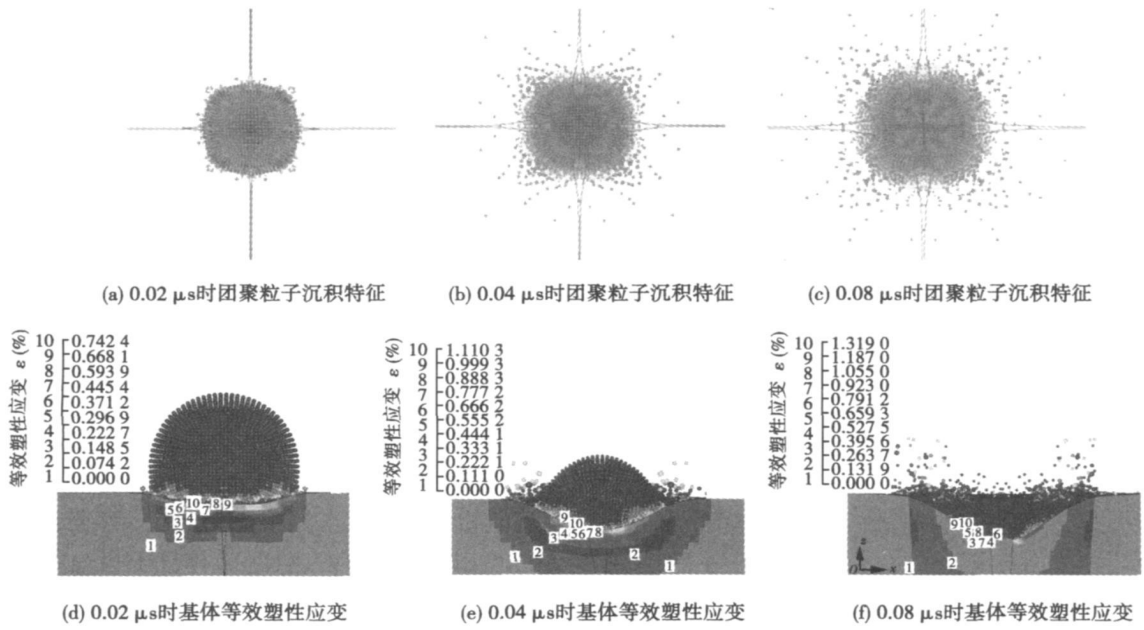


图 2 团聚粒子沉积特征与塑性应变

Fig 2 Deposition characteristics and plastic strain of agglomerate particle

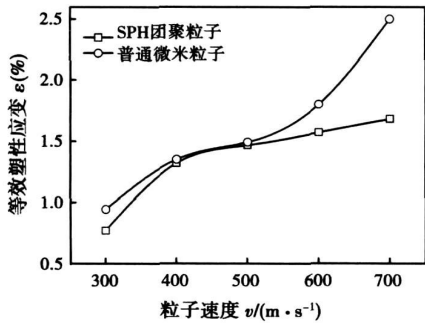


图 3 不同类型粒子的等效塑性应变

Fig. 3 Effective plastic strain of different particles

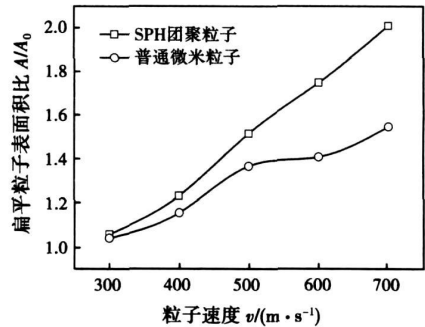


图 4 粒子碰撞面积比

Fig. 4 Area ratio of different flatten particles

积时的面积特征, 当纳米团聚粒子以不同速度撞击基体后, 粒子与基体交换能量的同时发生破碎. 当速度小于粒子沉积的临界速度时, 粒子与基体撞击的能量不足以使粒子发生破碎, 而当粒子速度高于临界速度时, 团聚粒子碰撞后的面积比与粒子速度之间存在一定的关系. 粒子碰撞后的面积说明粒子与基体之间发生了剧烈碰撞. 图中表明, 团聚粒子的沉积过程中, 粒子表面积的扩大系数要明显大于微米粒子的面积系数. 说明 SPH 粒子各单元之间失去相互作用, 碰撞应力受到杂化, 导致粒子对基体的碰撞能力下降, 并促使破碎面积增大.

3.4 金属团聚粒子沉积的界面特征

金属团聚粒子在沉积过程中, 为准确描述高速碰撞现象, 所选用的本构方程必须能表述材料在高

压强、温度和变形率下的复杂行为; 状态方程能够描述碰撞所导致的熔化以及汽化等相变过程. 材料在高应变率下的实际行为非常复杂, 难以用简单的状态方程来描述.

图 5 为 500 m/s 粒子对基体撞击能力的数值模拟. 喷涂过程中, 粒子与基体之间相互作用均产生了应变特征. 粒子在沉积过程与基体之间发生碰撞, 将出现粒子与基体之间的过渡层. 随着粒子速度的增大, 粒子与基体之间界面的过渡区域变得明显, 同时由于粒子的分作用力很大, 使得粒子产生了飞溅现象, 该现象随着粒子速度的增加而加剧.

3.5 团聚体内粒子的位移特征

图 6 给出了粒子在碰撞过程中粒子的最大位移, 表明呈团聚状的纳米粒子在喷涂过程中, 部分纳

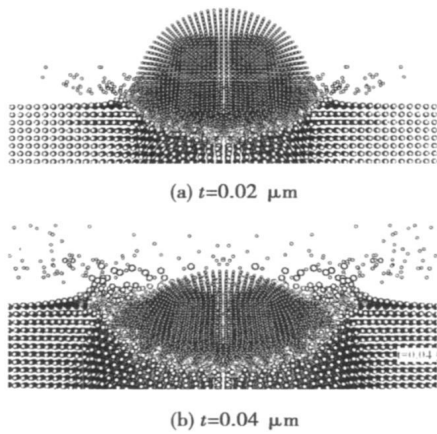


图5 不同时间粒子的沉积界面

Fig. 5 Depositing interface of agglomerate particle with different time

米粒子会侵入基体,使得粒子与基体之间存在金属相过渡区。因而,粒子的速度越高、温度越高,涂层与基体之间的过渡层面积越大,从而使得涂层与基体之间的结合越紧密。

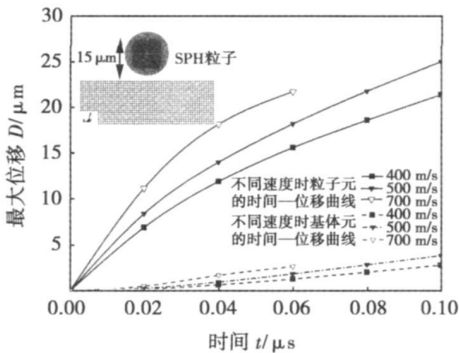


图6 粒子沉积的最大位移

Fig. 6 Maximum displacement of agglomerate particle

4 结 论

(1) 纳米粒子团聚到微米级粒子后,撞击基体时产生巨大的沉积应力,迫使自身与基体都产生变形。但粒子间松散状态导致粒子在碰撞基体时产生应力方向杂化,使得粒子对基体的撞击能力下降,同

时粒子将产生飞溅,破碎面积增大。

(2) 团聚粒子的塑性应变小于普通微米粒子,但团聚粒子的面积扩大比大于普通微米粒子。

参考文献:

- [1] Wilden J, Frank H. Thermal spraying-simulation of coating structure [C] // Lugscheider E. Proceedings of ITSC 2005, Basel, Switzerland, 2005; 287-292.
- [2] Barradas S, Molins R, Jeandin M. Laser shock flier impact simulation of particle-substrate interactions in cold spray [C] // Lugscheider E. Proceedings of ITSC 2005, Basel, Switzerland, 2005; 343-350.
- [3] Dykhuizen R C, Smith M F, Gilmore D L, *et al.* Impact of high velocity cold spray particles [J]. Journal of Thermal Spray Technology, 1999, 8(4): 559-564.
- [4] 李文亚, 李长久, 王豫跃, 等. 冷喷涂 Cu 粒子参量对其碰撞变形行为的影响 [J]. 金属学报, 2005, 41(3): 282-286.
Li Wenyu, Li Changjiu, Wang Yuyue, *et al.* Effect of parameter of cold sprayed Cu particles on its impacting behavior [J]. Acta Metallurgica Sinica, 2005, 41(3): 282-286.
- [5] 赵 铮, 李晓杰, 闫鸿浩, 等. 爆炸压实过程中颗粒碰撞问题的 SPH 法数值模拟 [J]. 高压物理学报, 2007, 21(4): 373-378.
Zhao Zheng, Li Xiaojie, Yan Honghao, *et al.* Numerical simulation of particles impact in explosive-driven compaction process using SPH method [J]. Chinese Journal of High Pressure Physics, 2007, 21(4): 373-378.
- [6] 楚锡华, 李锡夔. 颗粒材料的离散颗粒及间隙水渗流模型与数值模拟 [J]. 岩石力学与工程学报, 2006, 25(12): 2407-2416.
Chu Xihua, Li Xikui. A model of discrete particle and seepage of interstitial water in granular materials and numerical simulation [J]. Chinese Journal of Rock Mechanics and Engineering, 2006, 25(12): 2407-2416.
- [7] Hallquist J O. LS-DYNA theoretical manual [M]. USA: Livermore software Technology Corporation, 1998.
- [8] Yuan Xiaojing, Wang Hangong, Hou Genliang, *et al.* Numerical modeling of a low temperature high velocity air fuel spraying process with injection of liquid and metal particle [J]. Journal of Thermal Spray Technology, 2006, 15(3): 413-421.
- [9] Askeland Donald R, Phule P. The science and engineering materials fourth edition II [M]. 北京: 清华大学出版社, 2000.

作者简介: 侯根良, 男, 1970 年出生, 博士, 副教授, 主要从事特种材料开发研究, 发表论文 50 余篇。

Email: hougenliang@163.com

structured light image of weld seam

Elimination of gas holes of laser cladding on 2A12 aluminum alloys

SUN Fujuan (Qingdao Branch, Naval Aeronautical Engineering Academy, Qingdao 266041, Shandong, China). p93–96

Abstract: Laser cladding Al-Y (6%Y) was used to repair corrosion damage of 2A12 aluminum alloys. One group of the specimens was shocked on every deposited layer, the other was only deposited Al-Y (6%Y). After aging and fatigue test, fracture and element test were studied. The results show that the safety life of the shocked specimen is 871% of the specimens without shock and there was no pore in the deposited layer which is joined firmly with the substrate. There were many pores in the deposited layer of the specimens without shock, which lead to reduction of the safety life. The element test indicates that parts of the substrate is engaged in metallurgical procedure and the element Y is seriously burnt.

Key words: aluminum alloys; laser cladding; safety life; fatigue fracture

Experiment research on laser transmission welding of two different thermoplastics

WANG Xiao, YANG Kun, ZHANG Huizhong, LIU Huixia (School of Mechanical Engineering, Jiangsu University, Zhenjiang 212013, Jiangsu, China). p97–100

Abstract: The experiments on laser transmission welding of dissimilar plastic between transparent PS and PVC were carried out with cleanweld additive, and the welding quality was investigated by orthogonal test. Tensile and section tests were conducted for experimental samples, and the influence of welding factors on tensile strength and weld seam size were analyzed. The optimized welding parameters are obtained by range method, which indicates the influencing parameters on welding strength are welding speed, fixture pressure, beam diameter, laser average power, laser frequency, holding time after welding. Research results are helpful to guide practical production.

Key words: laser welding; polystyrene; polyvinylchloride; additive; transmission welding

Digital AC servo push & pull feeding system for CO₂ welding

YANG Shuai, LIU Jia, YAN Sibao, YIN Shuyan (College of Mechanical Engineering & Applied Electronics Technology, Beijing University of Technology, Beijing 100124, China). p101–104

Abstract: A push & pull feeding system with real-time control for CO₂ welding was proposed and achieved. It utilizes the motion controller to control AC servo motor with the low moment of inertia, fast response, and the buffer to connect the constant feeding part and the push & pull feeding part. The PWM feeder speed control circuit with speed negative feedback by rotate coder was designed to compensate the speed fluctuation caused by the system load and sup-

ply voltage changing. The push & puller feeding mechanism was designed to push & pull the wire based on the AC servo motor. According to the characteristics of CO₂ welding with push & pull feeding system, the feeder speed curve is pre-designed. The wire motion was managed by the real-time control software written in the motion controller. The system has good ability in anti-jamming and stability. The highest feeder frequency with push & pull process can reach 90 Hz.

Key words: AC servo motor; buffer; real-time control; push & pull feeding

SPH simulation on agglomerate Fe particle deposition in low temperature high velocity air fuel spraying process

HOU Genliang¹, XU Xin², YUAN Xiaojing¹ (1. The Second Artillery Engineering College 501 staff, Xi'an 710025, China; 2. The Second Artillery Equipment Research Institute, Beijing, 100085, China). p105–108

Abstract: In order to study the effect of the agglomerate metal particle on the coatings building-up, the agglomerate nano metal particle deposition characteristics with smoothed particle hydrodynamics (SPH) were simulated in low temperature high velocity air fuel (LTHVAF) thermal spraying process. The results show that the agglomerate particles are splashed when the agglomerate particles impact on the substrate. During the deposition process, the effective strain of agglomerate particle is larger than that of the micron particle, but the area ratio of the agglomerate particle is less. At the same time, the pervasion occurs when the metal particle impacts on the substrate, which increases with the particle velocity.

Key words: thermal spray; nano-agglomerate particle; deposition characteristics; numerical simulation

Numerical simulation of welding deformation of a large carriage side wall

YAN Junxia, WANG Jun, ZHAO Chenyang, LIU Limin (College of Materials, Hebei University of Science and Technology, Shijiazhuang 050018, China). p109–112

Abstract: The main welding deformation of railway carriage sidewall was welded buckling distortion, which was simulated by thermal elastic-plastic finite element method with analysis in several selected areas including continuous welds, plug welds and intermittent welds. The results show that the plug welding and intermittent welding are the main reason that induce buckling distortion of sidewall in which transverse stiffeners and longitudinal stiffeners are welded on the side-wall. The critical buckling load decreases obviously and the buckling distortion increases on the plate with a free boundary. The measured results of buckling distortion are in agreement with the simulation results. Thus a complete set of instruction can be received for the real processing.

Key words: carriage side-wall; numerical simulation; buckling distortion